Biosensors and Bioelectronics 26 (2011) 2053–2059

Contents lists available at ScienceDirect

Biosensors and Bioelectronics

journal homepage: www.elsevier.com/locate/bios

Nanostructured digital microfluidics for enhanced surface plasmon resonance imaging

Lidija Malic[a,c,d], Teodor Veres[c,d,*], Maryam Tabrizian[a,b,c,**]

[a] Biomedical Engineering Department, McGill University, Montreal, QC, Canada, H3A 2B4
[b] Faculty of Dentistry, McGill University, Montreal, QC, Canada, H3A 2B4
[c] Centre for Biorecognition and Biosensors, Montreal, QC, Canada, H3A 2B4
[d] Industrial Materials Institute-NRC, Boucherville, QC, Canada, J4B 6Y4

ARTICLE INFO

Article history:
Received 16 June 2010
Received in revised form 30 July 2010
Accepted 1 September 2010
Available online 15 September 2010

Keywords:
Nanostructured digital microfluidics
Enhanced surface plasmon resonance
integrated electro-wetting on dielectric
with SPR imaging
DNA biochips

ABSTRACT

The advances in genomics and proteomics have unveiled an exhaustive catalogue of biomarkers that can potentially be used as diagnostic and prognostic indicators of genetic and infectious diseases. Current thrust in biosensor development is towards rapid, real-time, label-free and highly sensitive detection of the indicative biomarkers. While surface plasmon resonance imaging (SPRi) biosensors could potentially be the best suited candidate for biomarker-based diagnosis, important milestones need to be reached. Commercially available SPRi instrumentation is currently limited by the flow-cell technology to serial-sample processing and has limited sensitivity for the detection of markers present at low concentration. In this paper, we have implemented an approach to enhance sample handling and increase the sensitivity of the SPRi detection technique. We have developed a digital microfluidic platform with an integrated nanostructured biosensor interface that allows for rapid, ultra-low volume, sensitive, and automated on-chip SPRi detection of DNA hybridization reactions. Through the exploitation of electromagnetic properties of nanofabricated periodic gold nanoposts, SPRi signal was increased by 200% with the estimated limit of detection of 500 pM (90 attomoles). Using the versatile fluidic manipulation provided by the digital microfluidics, rapid and parallel target identification was achieved on multiple array elements within 1 min using 180 nL sample volume. By delivering multiple target analytes in individually addressable low volume droplets, without external pumps and fluidic interconnects, the overall assay time, cost and complexity was reduced. The proposed platform allows extreme versatility in the manipulation of precious low volume samples which makes this technology very suitable for diagnostic applications.
© 2010 Elsevier B.V. All rights reserved.

1. Introduction

The current thrust in biosensor development is towards real-time and label-free systems such as surface plasmon resonance (SPR). The potential of SPR as a label-free biosensor was recognized in the early 1980s. There are many commercial systems available on the market today with single channel, dual-channel or imaging capabilities (SPRi). As opposed to classical scanning angle or wavelength SPR systems, SPRi technology provides a CCD camera which detects variation in reflected light (differential image) and a sensogram that measures changes in reflectivity at a fixed angle. The combination of the two components allows for visualization of the entire biochip surface in real time and provides the means to monitor multiple interactions continuously and simultaneously without labels. This makes SPRi technique particularly attractive for the real-time monitoring of DNA hybridization reactions in an array format (Chen et al., 2007; Fiche et al., 2007; Lee et al., 2001; Livache et al., 2003; Manera et al., 2008). While SPRi appears to possess many of the desired characteristics for a DNA hybridization sensor, there are yet many challenges to overcome. In particular, commercially available SPRi instrumentation is limited by the flow-cell technology to serial-sample processing and has limited sensitivity for the detection of markers present at low concentration. To address these limitations, the research effort has focused on the use of novel microfluidic and nanotechnology tools to increase the capability of SPRi-based detection. Microfluidic devices have been employed to increase the throughput of SPRi biosensors (Eddings et al., 2009; Kanda et al., 2004; Lee et al., 2001, 2007; Liu et al., 2009; Luo et al., 2008; Malic et al.,

* Corresponding author at: Industrial Materials Institute-NRC, Boucherville, QC, Canada, J4B 6Y4. Tel.: +1 450 641 5232; fax: +1 450 641 5105.
** Corresponding author at: Biomedical Engineering Department, McGill University, 3775 University Street, Montreal, QC, Canada, H3A 2B4. Tel.: +1 514 398 8129; fax: +1 514 398 7461.
E-mail addresses: Maryam.Tabrizian@mcgill.ca (M. Tabrizian), Teodor.Veres@cnrc-nrc.gc.ca (T. Veres).

0956-5663/$ – see front matter © 2010 Elsevier B.V. All rights reserved.
doi:10.1016/j.bios.2010.09.001

Table 1
DNA sequences.

Probe	5′-/HS-C6/-GCG GCA TGA ACC GGA GGC CC-3′
Target	3′-CGC CGT ACT TGG CCT CCG GG-5′
Control	3′-TTA CGT ACA GTG TCC GCC CT-5′

The probe oligonucleotide used as a surface bound capture probe contains a C6 linker and a thiol modification at the 5′ end for grafting to the gold layer functionalized surface.

2009a; Ouellet et al., 2010; Wegner et al., 2002, 2004; Wheeler et al., 2004), while colloidal-gold nanoparticles (Fang et al., 2006; He et al., 2000; Lee et al., 2006; Lyon et al., 1998) and surface-bound nanostructures (Byun et al., 2005, 2006, 2007; Chen et al., 2004; Kim, 2006; Kim et al., 2006; Malic et al., 2007, 2009c) have been explored to amplify the SPRi signals. These two technologies offer many benefits to SPRi-based detection, including low-volume multichannel fluidic interfacing required by the SPR imaging format and significant signal amplification that allows microarray detection in low pM range. To date, the coupling of microfluidics and nanoparticle-based SPRi amplification mainly focused on the combination of continuous-flow microfluidic devices and colloidal-gold nanoparticles used as labels (Luo et al., 2008). An advantage of this approach is higher degree of assay automation provided by the microfluidic technology and increased SPRi signal due to strong interactions between localized and propagating surface plasmons in the presence of gold nanoparticles. A disadvantage is however the requirement for external fluidic pumps which control two-dimensional fluid flow and the transformation of label-free SPRi technique into a labelled-one by the nanoparticle tags. In this article, we present a new configuration for label-free SPRi detection of biomolecular binding interactions through the use of integrated nanostructured digital microfluidic platform that provides programmable, two-dimensional fluidic interface and reproducible electromagnetic field enhancement while retaining the benefit of label-free SPRi detection. While the previously developed digital microfluidic platform was shown to be compatible with SPRi for monitoring the bulk medium index change (Malic et al., 2009a) and employed for DNA immobilization in combination with off-chip SPRi detection (Malic et al., 2009b) we developed herein the sensing protocol tailored to on-chip droplet-based SPRi kinetic monitoring of DNA hybridization reaction. Additionally, we modified the digital microfluidic platform using electron-beam lithography to integrate an array of periodic gold nanostructures at the biosensor interface in order to enhance the SPRi signal and increase the detection sensitivity.

2. Experimental procedures

2.1. Chemicals and reagents

Heptadecafluoro-1-decanethiol (HDFT), >99.0% (Fluka), potassium phosphate dibasic solution, 1 M, pH 8.9 (1 M K_2HPO_4), Tris–EDTA buffer solution, pH 8.0 (TE buffer), sodium chloride (NaCl), sodium hydroxide (NaOH) and ethanol were all purchased from Sigma–Aldrich (St. Louis, MO, USA). All oligonucleotide (ODN) sequences (Table 1) were purchased from Integrated DNA Technologies (Coralville, IA, USA).

2.2. Design and setup

The EWOD platform shown in Fig. 1a and b is similar to the one described previously (Malic et al., 2009a), and consists of two parallel glass plates separated by 75 μm thick spacers. The top plate serves as the SPRi-biochip and is comprised of a gold ground electrode coated with a thin Teflon film. Teflon is patterned to define four circular detection spots. The detection spots for the standard EWOD top plate are 300 μm in diameter and comprise 50 nm thick uniform gold film. The nanostructured detection spots (nano-spots) are 800 μm in diameter and integrate periodic gold nanostructures residing on 50 nm gold underlayer. The bottom plate, containing the reservoir and transport (path) electrodes, also houses the dedicated detection electrodes which are aligned with the aforementioned detection spots. Adjacent to them on each side is a pair of actuation electrodes to facilitate and promote mixing. A dielectric layer, which is coated with Teflon, insulates the electrodes. Each electrode is independently actuated using a software-controlled switching electronic unit connected to the voltage source. The SPRi measurements are achieved by mounting the EWOD microfluidic chip onto the chip alignment stage and adjusting its position to couple it with the SPRi prism using index matching oil.

2.3. EWOD chip fabrication

The EWOD microfluidic chip was fabricated using a combination of micro- and nanofabrication techniques. The fabrication method previously described (Malic et al., 2009b) was adapted to allow nanopatterning of the biosensor surface comprising an array of periodic gold nanoposts. A brief review of the chip fabrication process, including the integration of nanostructures within the detection spots of the EWOD top plate, is provided in Supplementary Information S1.

2.4. Droplet manipulation

The droplets were formed from either the immobilization solution (1 M K_2HPO_4) or the hybridization buffer solution (1 M NaCl in TE buffer) for the DNA immobilization and DNA hybridization, respectively. The reservoirs were filled by dispensing ~0.5 μL drops of solution on the chip before aligning and clamping the bottom and top plates together. For all experiments, the EWOD medium surrounding the droplets was air. The droplets of ~90 nL were created on-chip from the reservoirs and manipulated by sequentially applying a positive DC potential of 90 V on the electrodes with 100 ms switching time. A Lab View custom-made computer program that controls the switching electronic circuit allowed programming of the droplet path and protocol automation.

2.5. DNA probe immobilization

On-chip DNA immobilization protocol was performed as described previously (Malic et al., 2009b). Briefly, the droplets containing 1 μM DNA probe (Table 1) in immobilization buffer were dispensed from the reservoirs and transported to the detection spots, where they were left stationary at 0 V for 3 h in humid environment to allow the thiolated DNA probes to covalently attach to gold. Following the probe immobilization, the top plate was removed and the detection spots were passivated with 20 mM HDTF in ethanol for 10 min to prevent unspecific target adsorption to the gold surface.

2.6. SPRi detection setup

SPRi detection was performed at room temperature using a custom made SPRi instrument comprising an 800 nm LED source and a CCD camera (GenOptics, France) placed in Memmert Peltier cooled incubator (Rose Scientific, Canada) for temperature control. Reflected intensity was displayed as a function of angle in the plasmon curve diagram. The slope of the plasmon curves was automatically computed to facilitate the selection of the working angle (θ_w) for kinetic analysis, which corresponded to the point of the plasmon curve at which the slope was maximized. In kinetic analysis, the reflected intensity (%R) was traced as a function of time

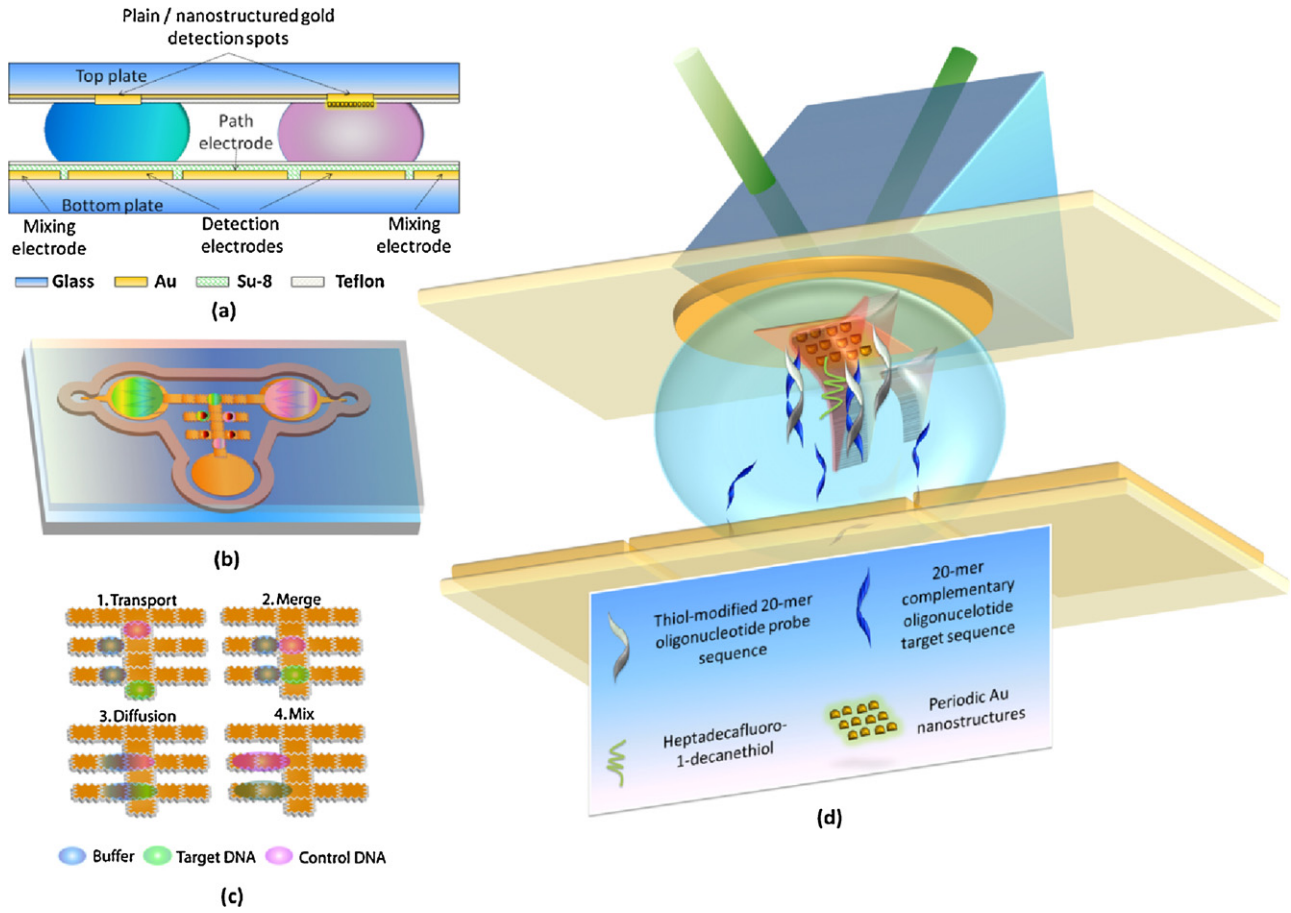

Fig. 1. Schematic of EWOD chip: (a) vertical cross-section, and (b) 3D layout; (c) schematic of assay protocol for SPRi detection of DNA hybridization using EWOD droplet manipulation; (d) schematic of nanostructured digital microfluidic chip coupled to SPRi.

allowing the monitoring of the DNA–DNA binding kinetics. The SPRi difference images captured by the CCD camera were recorded to obtain real-time information about the reactions occurring at the surface of the chip. The binding event was seen as an increase in the reflected intensity, characterized by a bright spot, which is easily distinguishable from the dark background.

2.7. EWOD protocol for SPRi detection of DNA hybridization

Specificity of droplet-based DNA hybridization reactions performed using the EWOD device was characterized with a standard EWOD top plate comprising 50 nm thick, 300 μm-diameter flat gold detection spots (see Supplementary Information, S1). Prior to the SPRi monitoring of binding reactions, the three reservoirs were filled with the hybridization buffer, 500 nM complementary target DNA and 500 nM mismatched control sequence (Table 1). The top plate was then assembled with the bottom plate by aligning the detection spots with the dedicated detection electrodes and inserted into the SPRi. To monitor the SPRi signal, four droplets (two buffer droplets, DNA target and DNA control droplets) were dispensed and displaced sequentially according to the protocol shown in Fig. 1c. Initially, two buffer droplets were dispensed and positioned onto the two detection spots. Following the acquisition of the plasmon curves and the selection of θ_w (Section 2.6), the baseline signal of kinetic analysis was obtained for each spot. After stable baseline, the sample droplets, containing the DNA target and the control DNA were dispensed and merged with the buffer droplets located on the detection spots. The transport of the sample droplets and subsequent merging with the buffer droplets was performed while keeping the detection electrodes activated in order to avoid the kinetic signal instability (Malic et al., 2009a). Complete droplet mixing was achieved by applying a pulsed voltage on the mixing electrodes for 60 s, resulting in final DNA target concentration of 250 nM. The kinetic measurements were performed three times to confirm the reproducibility of the experiment. After each experiment, the chip was taken out of the SPRi assembly and the surface was regenerated using 50 mM NaOH wash.

Similarly, the protocol for the enhanced SPRi detection of DNA hybridization was performed using the nanostructured EWOD top plate (to assess the corresponding SPRi signal amplification (Fig. 1d)). The response of the nanostructured detection area spot (nano-spot) was compared to that of a control spot (uniform 50 nm thick gold film) for the simultaneous DNA target hybridization at both probe regions. This was achieved by merging and mixing DNA target droplets, 500 nM or 1 nM in concentration, with the buffer droplets located at the detection spots, resulting in final target concentrations of 250 nM or 500 pM, respectively. Kinetic measurements were performed at fixed incidence angles for each plasmon curve, θ_{w_gold} and θ_{w_nano}, corresponding to the angle of maximum slope for uniform gold spot and nanostructured spot, respectively.

3. Results

3.1. Optimization of the nanostructured substrates: modeling and fabrication

Rigorous coupled wave analysis (RCWA) was employed to model the response of the nanostructured substrate for the

DNA hybridization event and compute the corresponding signal enhancement as described in the Supplementary Information S2. The parameters of the periodic nanopost structures (width, w = 50 nm and period, Λ = 110 nm) were previously optimized to yield maximum signal enhancement, which occurred at the nanopost height h = 30 nm and initial Au film thickness t = 20 nm (Malic et al., 2007). However, due to the fabrication constraints, the minimum underlayer gold film thickness (t) required for successful and reproducible nanostructure fabrication was found to be 50 nm. At lower t values, the adhesion of the gold film was not sufficiently strong to withstand the lift-off process, resulting in a poorly defined nanostructured interface. The effect of t on the enhancement with respect to the nanopost height (h) was investigated numerically by varying the two parameters from 0 to 60 nm and 10 to 100 nm, respectively, at a constant w and Λ values. The sensitivity enhancement factor SEF was defined as the ratio of resonant angle shift due to DNA hybridization event (assuming a saturated surface comprising fully formed duplexes (Elhadj et al., 2004)) on a nanostructured surface to that of a conventional SPR structure (uniform 50 nm-thick gold film) used as control. From Fig. 2a, the enhancement was observed for h not exceeding 30 nm for all t values; above which the control provided better sensitivity. For t = 50 nm, the maximum sensitivity (SEF = 3.21) was obtained at h = 30 nm. These values were then used for the fabrication of the nanostructures (see Supplementary Information). Fig. 2b shows a sample SEM image of the nanopost structures of nominally circular shape with Λ = 110 nm and $w = 50 \pm 2$ nm.

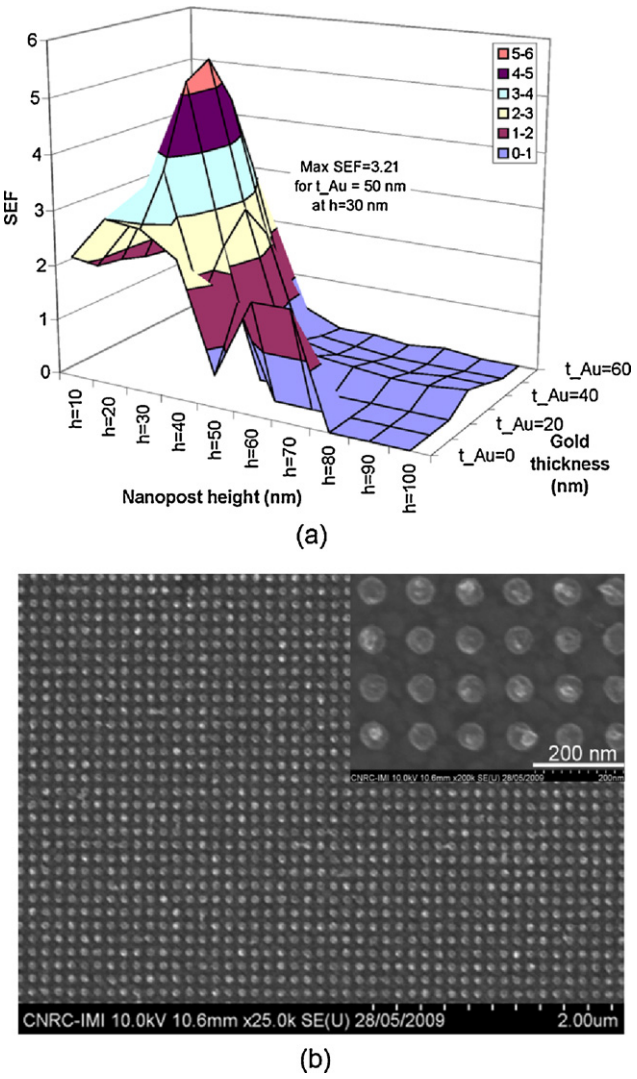

Fig. 2. (a) Numerically obtained SEF for nanostructured SPR substrate with nanoposts of different height and underlayer gold film thickness; (b) SEM micrograph showing the fabricated nanostructures.

3.2. Parallel SPRi detection of DNA hybridization: specificity assay

Gold surface functionalization was dynamically achieved with the inherent flexibility of EWOD, which allowed for electronic control of droplet generation and positioning to the selected detection spot, where the thiolated DNA self-assembled without an applied potential. Following the surface passivation, the binding specificity of a fully matched DNA target sequence and a mismatched control DNA sequence with the immobilized DNA probes was conducted to obtain the plasmon and kinetic curves as described in Section 2.7. Fig. 3a shows the plasmon curves for the two spots in the hybridization buffer medium. Both curves exhibited similar characteristics with identical resonance angles (θ_R = 55.11°), confirming the uniformity of the gold film across the sample and the reproducibility in the immobilized DNA probe density. Following the selection of θ_w = 56.02°, the kinetic signals of the DNA hybridization reaction were monitored simultaneously for the two spots by merging and mixing with the target DNA and the control DNA sequence droplets. Consequently, the specificity of the DNA target binding could be evaluated instantaneously from Fig. 3b using the random DNA sequence as a control. The time required to reach the kinetic signal saturation corresponded to 14–16 min of the DNA hybridization reaction, with the estimated adsorption rate constant $k_a = 4.4 \times 10^3\ M^{-1}\ s^{-1}$.

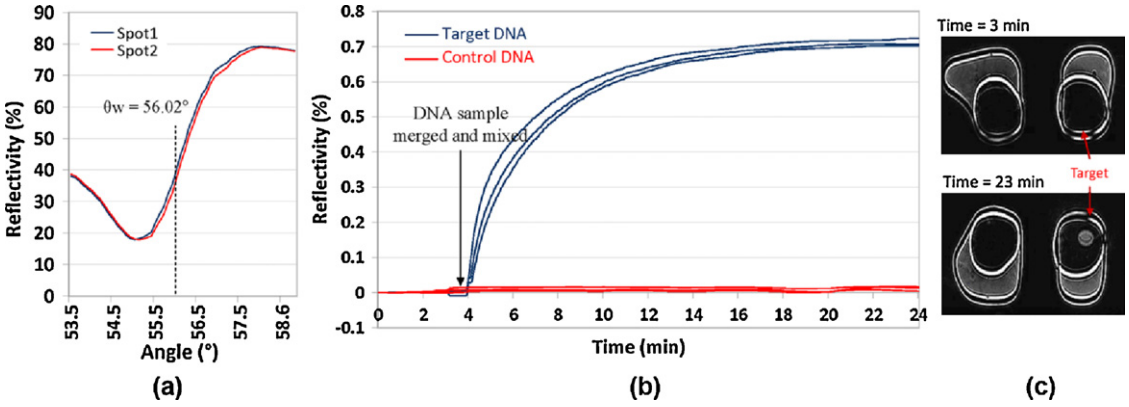

Fig. 3. SPRi monitoring of DNA hybridization reaction for target DNA and control DNA sequences: (a) SPRi plasmon curve plots of reflectivity (%) vs. angle (°), (b) kinetic curve plots of reflectivity (%) vs. time (min), and (c) SPRi difference images of binding reactions.

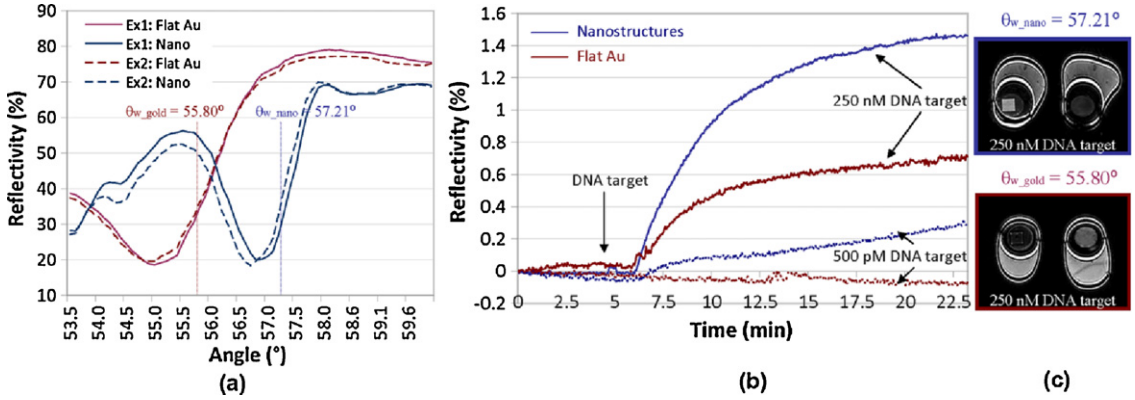

Fig. 4. SPRi monitoring of target DNA hybridization reaction on a nanostructured biosensor interface compared to uniform gold spot (control): (a) SPRi plasmon curve plots of reflectivity (%) vs. angle (°), (b) SPRi kinetic curve plots for DNA target concentration of 250 nM and 500 pM. The control was measured at the working angles which maximizes the plasmon curve of flat gold substrate (θ_{w_gold} = 55.80°), and the nanostructure sample response was measured at the working angle which maximizes the plasmon curve of the nanostructured substrate (θ_{w_nano} = 57.21°), and (c) difference images of 250 nM DNA target hybridization at each θ_w.

3.3. Nanostructure-enhanced SPRi detection of DNA hybridization

SPRi detection of DNA hybridization was performed using the EWOD platform with integrated nanostructured SPR substrate by comparing the response of a nano-spot to that of control. To assess the nanostructure-based amplification of the DNA hybridization signal and the corresponding limit of the detection, two experiments were performed on two different samples using final DNA target concentrations of 250 nM and 500 pM. The plasmon curves of control spots and nano-spots for the two samples in buffer media are shown in Fig. 4a. For each experiment, the working angle was sequentially chosen at the maximum slope of each plasmon curve to ensure maximum kinetic signal for each spot. Hence, SPRi kinetic measurements were performed at working angles which corresponded to θ_{w_gold} = 55.8° (Ex1) and θ_{w_nano} = 57.1° (Ex2) for control spot and nano-spot, respectively.

In each experiment, the kinetic signals of the DNA hybridization reaction were monitored simultaneously for the two spots by merging and mixing the DNA target droplet with the buffer. The kinetic curves and the difference images of the target binding to the control spot and nano-spot at their corresponding working angles are shown in Fig. 4b and c, respectively. The nano-spot provided two-fold signal amplification compared to control within 16 min of the DNA hybridization reaction, and reduced the time required for correct target identification to 60 s only. The estimated limit of detection for the nanostructured interface corresponded to a concentration of 500 pM target DNA, which is approximately an order of magnitude improvement compared to control.

4. Discussion

SPRi kinetic measurements of the biomolecular binding interactions were reported for the first time using an integrated digital microfluidic platform. Assay protocol that differed from a typical standard flow cell-based assay was developed first to allow for the integration of the EWOD-based fluidic processing and SPR imaging and validated for DNA hybridization reactions. In a traditional, flow-cell-based SPRi hybridization assay, the DNA–DNA binding kinetics are monitored for continuously flowing buffer or sample solutions, which are interchanged using external fluidic injection loops to avoid interruption in the liquid flow. Conversely, SPRi detection coupled to the digital microfluidic platform relied on the 'stop-flow' condition for target delivery using discrete sample droplets. As continuous sample interchange was impossible, the paths of buffer and sample droplets were sequentially programmed to merge at specified time intervals in order to allow for the kinetic measurement of the binding reactions. The stability of the kinetic signals (Figs. 3b and 4b) during droplet merging was ensured through continuous wetting of the detection spot surface by keeping the detection electrodes activated. This aimed at avoiding significant change in bulk refractive index which would otherwise occur if the surface became exposed to air and would consequently drown the small refractive index change due to DNA hybridization. In addition, the device was designed to enhance the initial diffusion limited mixing of the merged droplets via mixing electrodes (Fig. 1d) and subsequently increase the kinetic rates of binding reactions. From Fig. 3b and c, the use of active mixing in EWOD device allowed for the identification of DNA target binding within first 2 min of the DNA hybridization reaction (signal to noise ratio, SNR > 3). The reaction was specific and the surface could be easily regenerated without any significant signal loss. The time required to reach signal saturation (~14–16 min) was longer than that typically obtained using a standard flow cell (5–8 min, $k_a \sim 1 \times 10^4\ M^{-1}\ s^{-1}$) (Lee et al., 2006). However, the sample consumption was decreased by more than 3 orders of magnitude (180 nL compared to 700 μL–1 mL of the sample consumed in a typical hybridization assay using a flow cell). The tradeoff between the total sample volume consumption and the speed of reaction kinetics was due to the inverse scaling of the reaction time to total available target concentration (Lee et al., 2006). Compared to the flow-cell technology, the low sample volume consumed by EWOD device resulted in a decrease of the absolute target concentration, which consequently increased the time required to reach steady-state target surface coverage. Additionally, as in other "stop-flow" devices, the binding reactions on an EWOD platform were mostly diffusion-limited and thus exhibited slower binding kinetics than the flow-cell technology capable of high-flow rates and continuous surface replenishment (Schasfoort and Tudos, 2008). It is noteworthy, however, that the binding rate of negatively charged DNA target may be enhanced using the electric interface of an EWOD device to apply a positive potential at the biosensor surface, similarly to that demonstrated for the DNA probe immobilization (Malic et al., 2009b). Another advantage of the proposed system for SPRi biosensing applications lies in its flexibility and versatility; the same device was employed for both, target sample delivery and reproducible probe immobilization without any change in device configuration. Finally, the use of EWOD platform for SPRi biosensing applications allowed monolithic integration of nanostructured interface to increase the sensitivity of SPRi detection. The exploitation of metallic nanostructures allows strong optical coupling of incident light to localized surface plasmons (LSPs), accompanied by electromagnetic field enhancements which are used in surface-

enhanced SPR and SPRi (Byun et al., 2005, 2006, 2007; Kim, 2006; Kim et al., 2006; Malic et al., 2007, 2009c). Herein, the sensitivity enhancement is attributed to strong interactions between localized surface plasmons, propagating surface plasmons, and binding biomolecules, which leads to a change in the resonance conditions and consequently to an additional shift of resonance angle and reflectivity. In order to demonstrate the nanostructure-based SPRi signal amplification for the DNA hybridization event and to evaluate the corresponding limit of detection using the digital microfluidic platform, we compared the response of nano-spot to that of control on two different samples. As can be seen in Fig. 4a, the shape of the plasmon curves and the position of the plasmon peak (θ_R) were almost identical for the control spots of the two samples. The small differences in the θ_R for the nano-spots were due to the fabrication-induced sample-to-sample variation in the nanostructure geometry. From Fig. 4b, the hybridization kinetics on the control spot for the 250 nM DNA target concentration were similar to those obtained using the standard top plate. Conversely, for the nano-spot, the kinetic signal progressively increased resulting in signal amplification of more than 200% after 16 min of hybridization reaction. This enhancement was also easily observed by comparing the difference images shown in Fig. 4c, whereas the nanostructured spot exhibited increased contrast and a brighter image. Consequently, this increase in the SPRi signal response resulted in a decrease in the time required to correctly identify the DNA target to 1 min only. Nevertheless, the experimental signal enhancement, which strongly depends on the dielectric medium in contact with the gold surface (Malic et al., 2009c; Yoon and Kim, 2008), was lower than the numerically predicted SEF value. This can be attributed to the higher value assumed for the modeled refractive index change in comparison to the actual experimentally obtained value for the DNA hybridization event. The model value corresponded to a saturated surface comprising fully formed duplexes (Elhadj et al., 2004), which overestimated experimental conditions, considering that the ideal duplex monolayer could not be formed within 15 min of the DNA hybridization reaction at the evaluated target concentration (250 nM in total volume of 180 nL or 45 femtomoles). Nevertheless, the integrated nano-spots exhibited an order of magnitude increase in limit of detection, allowing correct DNA target identification in sub-nM concentrations (as low as 90 attomoles) (Fig. 4b). At this low target concentration, the surface signal was limited by both adsorption kinetics and diffusion to the surface (Lee et al., 2006) such that signal saturation was not reached even after 16 min of the hybridization reaction. The signal enhancement can be further increased by optimizing the EBL fabrication process to allow nanostructure fabrication on a thinner underlayer gold film, for instance $t = 20$ nm (Malic et al., 2007). In the present work, a 50 nm thick underlayer gold film was required to achieve sufficiently strong adhesion with the structural gold film (nanostructured features) to withstand the resist liftoff process. This subsequently affected the SPR signal as predicted by the numerical model (Fig. 2a). Conversely, nanoimprint lithography could potentially overcome the limitations of EBL by completely alleviating the need for multiple gold depositions and sensitive fabrication procedures such as lift-off (Malic et al., 2009c). The integration of nano-imprinted polymeric substrates with EWOD for SPRi biosensor applications may provide reproducible, low-cost solution for rapid and sensitive detection of DNA hybridization.

5. Conclusion

The digital microfluidic technology with integrated nanostructured biosensor interface was employed to create a droplet-based microarray SPRi system for ultra-low volume, sensitive detection of DNA hybridization. A protocol was developed to allow kinetic analysis of DNA hybridization reactions on planar and nanostructured gold surfaces using electrowetting-on-dielectric droplet actuation. The kinetic measurements were performed under stop-flow conditions while active mixing was initiated using EWOD actuation to decrease the assay time. Signal saturation on uniform gold surfaces was observed after 14–16 min of the DNA hybridization reaction, while sample consumption was decreased by more than three orders of magnitude compared to the standard DNA hybridization assay that employs the flow cell technology. The nanostructured biosensor interface was integrated with the EWOD platform to achieve increased sensitivity of SPRi detection. The optimized 50 nm diameter nanoposts with a period of 110 nm and 50 nm gold underlayer were incorporated with the detection spots of the EWOD top plate. The DNA hybridization signal was increased by 200% for the nanostructured substrate allowing rapid target identification within only 60 s of the reaction. The limit of detection was estimated to be 500 pM for 10 min of DNA hybridization, which translates to 90 attomoles DNA molecule detection in 180 nL droplets. Although only four detection spots were employed in the present study, the straightforward surface functionalization, coupled with the unique design flexibility of EWOD for high-density electrode fabrication are attractive features for a high-throughput implementation of the concept, which is the subject of ongoing work in our laboratory. Coupled with SPRi, nanostructured EWOD biochip platforms promise to dramatically increase the sensitivity and speed of biomolecule's detection beyond DNA biosensors, finding its application in both research and clinical settings.

Acknowledgements

The authors thank le Fonds québécois de la recherche sur la nature et les technologies (FQRNT) for the scholarship, FQRNT-team grant, FQRNT-Centre for Biorecognition and Biosensors, Genome Quebec, Genome Canada, Natural Sciences and Engineering Council of Canada, NanoQuebec and the Industrial Materials Institute of National Research Council of Canada for their financial support. We thank Francois Normandin for his contribution in building the control software and switching electronic, Dr. Daniel Brassard for his help with the dielectric film fabrication process and Dr. Bo Cui for his help with the development of the nanostructured interface.

Appendix A. Supplementary data

Supplementary data associated with this article can be found, in the online version, at doi:10.1016/j.bios.2010.09.001.

References

Byun, K., Kim, S., Kim, D., 2005. Optics Express 13 (10), 3737–3742.
Byun, K.M., Kim, D., Kim, S.J., 2006. Sensors and Actuators B: Chemical 117 (2), 401–407.
Byun, K.M., Yoon, S.J., Kim, D., Kim, S.J., 2007. Optics Letters 32 (13), 1902–1904.
Chen, S.J., Chien, F.C., Lin, G.Y., Lee, K.C., 2004. Optics Letters 29 (12), 1390–1392.
Chen, W.Y., Hu, W.P., Su, Y.D., Taylor, A., Jiang, S., Chang, G.L., 2007. Sensors and Actuators B: Chemical 125 (2), 607–614.
Eddings, M.A., Eckman, J.W., Arana, C.A., Papalia, G.A., Connolly, J.E., Gale, B.K., Myszka, D.G., 2009. Analytical Biochemistry 385 (2), 309–313.
Elhadj, S., Singh, G., Saraf, R.F., 2004. Langmuir 20 (13), 5539–5543.
Fang, S., Lee, H.J., Wark, A.W., Corn, R.M., 2006. Journal of the American Chemical Society 128 (43), 14044–14046.
Fiche, J.B., Buhot, A., Calemczuk, R., Livache, T., 2007. Biophysical Journal 92 (3), 935–946.
He, L., Musick, M.D., Nicewarner, S.R., Salinas, F.G., Benkovic, S.J., Natan, M.J., Keating, C.D., 2000. Journal of the American Chemical Society 122 (38), 9071–9077.
Kanda, V., Kariuki, J.K., Harrison, D.J., McDermott, M.T., 2004. Analytical Chemistry 76 (24), 7257–7262.
Kim, D., 2006. Journal of the Optical Society of America A: Optics and Image Science 23 (9), 2307–2314.
Kim, K., Yoon, S.J., Kim, D., 2006. Optics Express 14 (25), 12419–12431.
Lee, H.J., Goodrich, T.T., Corn, R.M., 2001. Analytical Chemistry 73 (22), 5525–5531.
Lee, H.J., Wark, A.W., Corn, R.M., 2006. Langmuir 22 (12), 5241–5250.

Lee, K.-H., Su, Y.-D., Chen, S.-J., Tseng, F.-G., Lee, G.-B., 2007. Biosensors and Bioelectronics 23 (4), 466–472.
Liu, J., Eddings, M.A., Miles, A.R., Bukasov, R., Gale, B.K., Shumaker-Parry, J.S., 2009. Analytical Chemistry 81 (11), 4296–4301.
Livache, T., Maillart, E., Lassalle, N., Mailley, P., Corso, B., Guedon, P., Roget, A., Levy, Y., 2003. Journal of Pharmaceutical and Biomedical Analysis 32 (4–5), 687–696.
Luo, Y.Q., Yu, F., Zare, R.N., 2008. Lab on a Chip 8 (5), 694–700.
Lyon, L.A., Musick, M.D., Natan, M.J., 1998. Analytical Chemistry 70 (24), 5177–5183.
Malic, L., Veres, T., Tabrizian, M., 2009a. Lab on a Chip 9 (3), 473–475.
Malic, L., Veres, T., Tabrizian, M., 2009b. Biosensors and Bioelectronics 24 (7), 2218–2224.
Malic, L., Cui, B., Veres, T., Tabrizian, M., 2007. Optics Letters 32 (21), 3092–3094.
Malic, L., Cui, B., Tabrizian, M., Veres, T., 2009c. Optics Express 17 (22), 20386–20392.
Manera, M.G., Spadavecchia, J., Leone, A., Quaranta, F., Rella, R., Dell'atti, D., Minunni, M., Mascini, M., Siciliano, P., 2008. Sensors and Actuators B: Chemical 130 (1), 82–87.
Ouellet, E., Lausted, C., Lin, T., Yang, C.W.T., Hood, L., Lagally, E.T., 2010. Lab on a Chip 10 (5), 581–588.
Schasfoort, R.B.M., Tudos, A.J., 2008. Handbook of Surface Plasmon Resonance. RCS Publishing, Cambridge, UK.
Wegner, G.J., Lee, H.J., Corn, R.M., 2002. Analytical Chemistry 74 (20), 5161–5168.
Wegner, G.J., Wark, A.W., Lee, H.J., Codner, E., Saeki, T., Fang, S., Corn, R.M., 2004. Analytical Chemistry 76 (19), 5677–5684.
Wheeler, A.R., Chah, S., Whelan, R.J., Zare, R.N., 2004. Sensors and Actuators B: Chemical 98 (2–3), 208–214.
Yoon, S.J., Kim, D., 2008. Journal of the Optical Society of America A: Optics and Image Science 25 (3), 725–735.